Science of the Total Environment 727 (2020) 138488

Contents lists available at ScienceDirect

Science of the Total Environment

journal homepage: www.elsevier.com/locate/scitotenv

Characterization of radioactive particles from the Dounreay nuclear reprocessing facility

Ian Byrnes [a,*], Ole Christian Lind [a], Elisabeth Lindbo Hansen [a,b], Koen Janssens [c], Brit Salbu [a]

[a] Center for Environmental Radioactivity (CERAD CoE), Faculty of Environmental Sciences and Natural Resource Management, Norwegian University of Life Sciences (NMBU), P.O. Box 5003, 1433 Ås, Norway
[b] Norwegian Radiation and Nuclear Safety Authority (DSA), P.O. Box 329, Skøyen, NO-0213 Oslo, Norway
[c] AXES, Department of Physics, University of Antwerp, Groenenborgerlaan 171, B-2020 Antwerp, Belgium

HIGHLIGHTS

- Multi-technique characterization of radioactive Dounreay (MTR and DFR) particles
- Particle characteristics reflect nuclear fuel designs and accidental release scenarios.
- Highly enriched ($^{235}U/^{238}U$ range of 2.2–4.0), tetravalent U in both particle types
- Particles from MTR (Al, Nd ~ 1–2 atom %) can be differed from DFR (Nb, Mo ~ 0.5–1 atom %).
- Beta emission derived dose rates for Dounreay particles support existing models.

GRAPHICAL ABSTRACT

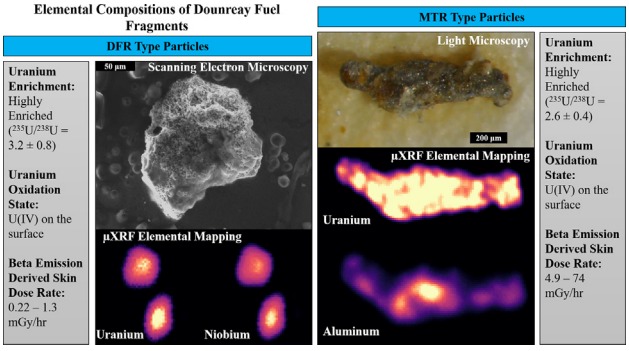

ARTICLE INFO

Article history:
Received 22 December 2019
Received in revised form 2 April 2020
Accepted 4 April 2020
Available online 7 April 2020

Editor: Kevin V. Thomas

Keywords:
Uranium particles
Electron microscopy
Micro-XRF
Micro-XANES
Contact dosimetry
Dounreay

ABSTRACT

Radioactive particles originating from nuclear fuel reprocessing at the United Kingdom Atomic Energy Authority's Dounreay Facility were inadvertently released to the environment in the late 1950s to 1970s and have subsequently been found on site grounds and local beaches. Previous assessments of risk associated with encountering a particle have been based on conservative assumptions related to particle composition and speciation. To reduce uncertainties associated with environmental impact assessments from Dounreay particles, further characterization is relevant.

Results of particles available for this study showed variation between Dounreay Fast Reactor (DFR) and Materials Test Reactor (MTR) particles, reflecting differences in fuel design, release scenarios, and subsequent environmental influence. Analyses of DFR particles showed they are small (100–300 µm) and contain spatially correlated U and Nb. Molybdenum, part of the DFR fuel, was identified at atomic concentrations below 1%. Based on SR-based micrometer-scale X-ray Absorption Near Edge Structure spectroscopy (µ-XANES), U may be present as U (IV), and, based on a measured Nb/U atom ratio of ~2, stoichiometric considerations are commensurable with the presence of UNb_2O_7. The MTR particles were larger (740–2000 µm) and contained U and Al inhomogeneously distributed. Neodymium (Nd) was identified in atomic concentrations of around 1–2%, suggesting it was part of the fuel design. The presence of U(IV) in MTR particles, as indicated by µ-XANES analysis, may be related to oxidation of particle surfaces, as could be expected due to corrosion of UAl_x fuel particles in air. High $^{235}U/^{238}U$ atom ratios in individual DFR (3.2 ± 0.8) and MTR (2.6 ± 0.4) particles reflected the presence of highly enriched

* Corresponding author at: Norwegian University of Life Sciences, Center of Excellence for Environmental Radioactivity (CERAD), Faculty of Environmental Sciences and Natural Resource Management, P.O. Box 5003, 1433 Ås, Norway.
E-mail address: ian.byrnes@nmbu.no (I. Byrnes).

https://doi.org/10.1016/j.scitotenv.2020.138488

uranium. The DFR particles featured lower ^{137}Cs activity levels (2.00–9.58 kBq/particle) than the MTR (43.2–641 kBq ^{137}Cs/particle) particles. The activities of the dose contributing radionuclides ^{90}Sr/^{90}Y were proportional to ^{137}Cs (^{90}Sr/^{137}Cs activity ratio ≈ 0.8) and particle activities were roughly proportional to the size. Based on direct beta measurements, gamma spectrometry, and the VARSKIN6 model, contact dose rates were calculated to be approximately 74 mGy/h for the highest activity MTR particle, in agreement with previously published estimates.

1. Introduction

In nuclear fuel reprocessing, uranium (U) and plutonium (Pu) from spent nuclear fuel are recovered for civil or military uses. Essential to reprocessing is the dissolution of the spent fuel, a procedure that increases the potential for contaminant release in liquid waste discharges (Choppin et al., 2013). Reports on radioactive particles found in the vicinity of reprocessing sites indicate that the dissolution of fuel may be incomplete and that residual fuel fragments and particles in the discharges can give rise to radioactive particle contamination in the environment such as in the case of Krasnoyarsk-26, Sellafield, and Dounreay reprocessing facilities (Bolsunovsky et al., 2017; Dennis et al., 2007; Geckeis et al., 2019; Lind, 2006). Failure to recognize the presence of radioactive particles, defined by the International Atomic Energy Agency (IAEA) as "a localized aggregation of radioactive atoms that give rise to an inhomogeneous distribution of radionuclides significantly different from that of the matrix background", may have a number of serious consequences (IAEA, 2011). The presence of insoluble particles in bulk samples may cause incomplete dissolution, which may give rise to analytical inconsistencies, irreproducible results, and erratic conclusions (Cooper et al., 1994; Danesi et al., 2002; Oughton et al., 1993; Simon et al., 1995). Furthermore, there will be unacceptably large uncertainties associated with model predictions for dispersion and ecosystem transport as well as dose assessment (Bunzl, 1997; Darley et al., 2003). To characterize particle properties of relevance for impact assessments, however, a combination of advanced technologies are needed (Salbu et al., 1994; Salbu and Lind, 2020).

Particles have been identified as part of the radioactive contamination of many sites in addition to nuclear reprocessing facilities, such as from nuclear weapon tests, conventional detonation of nuclear weapons, fallout from nuclear reactor explosions or fires, and use of depleted uranium (DU) for ammunitions (Salbu et al., 2011). Research has demonstrated that the particle composition will depend on the source, while the release scenario will influence particle properties of relevance for environmental transfer. (Salbu and Lind, 2020). Particle structure and morphology, elemental composition, and oxidation state of U or Pu have been shown to be key parameters in determining potential subsequent weathering and remobilization in the ecosystem (Salbu, 2016).

Radioactive particles were identified at the Dounreay facility foreshore in November 1983 and have since been recovered at a rate of approximately eight particles per month from foreshore sediments at the United Kingdom Atomic Energy Authority's (UKAEA) former reactor research establishment at Dounreay (Fig. 1), Caithness, Scotland, and from the nearby Sandside (2.5 km west of site) and Dunnet (25 km east of site) public beaches (Tyler et al., 2010). These highly radioactive (MBq) particles and fragments are small pieces (typically 0.2–2 mm) of fuel material, formed and accidentally released to the marine environment during historical nuclear fuel reprocessing operations involving irradiated spent fuel, which took place during the late 1950s, 1960s, and 1970s (Henderson et al., 2007; Potter et al., 2003). Opened in 1955, the UKAEA Dounreay facility included three nuclear reactors, the Dounreay Fast Reactor (DFR), the Prototype Fast Reactor (PFR), and the Material Testing Reactor (MTR) along with fuel fabrication and reprocessing capabilities. A total activity of about 10 PBq was

Fig. 1. The location of Dounreay Site Restoration Ltd. with nearby public beaches shown.

discharged to the marine environment from the facility until decommissioning in 1994 (CEG, 1990). Studies of the extent of particle contamination were commissioned by Scottish Environmental Protection Agency (SEPA) in 1997 and coincided with the implementation of a fishing exclusion zone of 2 km around the facility as a result of foreshore particle finds (Dennis et al., 2007). Routine monitoring programs of facility grounds and local public beaches (Sandside, Murkle, and Dunnet) remain in place today (DSRL, 2019a; DSRL, 2019b; DSRL, 2019c).

As they are relatively small in size, these particles escaped the main filtration systems of the facility and were released via the low activity liquid effluent systems (the Low Activity Drain (LAD), Old Diffusion Chamber (ODC), and the Sea Tanks) into the surrounding marine environment (PRAG(D), 2012). This system, which was withdrawn from use in 1992, was connected to a discharge point on the seabed by sixteen 23 m long boreholes. The integrity of these boreholes failed some time prior to identification in 1981, creating a release pathway to the marine environment. This has been described in previous reports to be the primary pathway for particle releases, and efforts have been made to seal and prevent future releases (Henderson et al., 2007; PRAG(D), 2012). Other potential release pathways are minor, but include a fire in 1967 and an incident associated with a work shaft that was repurposed for solid waste storage (Dennis et al., 2007). The work shaft was originally built to support work on the active waste effluent system; it was modified and used for solid waste storage from 1958 to 1977. An explosion due to hydrogen build up occurred on May 10, 1977 (Henderson et al., 2007). Particle release via the shaft explosion may have occurred; however, groundwater pumping from the work shaft to the low activity liquid effluent system also occurred, as required for use as waste storage, making the specific source difficult to identify.

Released particles can be assumed to have spent years to decades in the marine environment. Modeling work has been performed to estimate the transport and numbers of particles released. Initial modeling predicted that the majority of particles would move northeast of the old diffuser (Henderson et al., 2007; Soulsby et al., 2006). More recent efforts compared the modeling work with seabed particle finds and confirmed that the discharge location around the ODC and LAD are the point of exit and that the particles have, generally, formed a plume traveling northeast and parallel to the shore (PRAG(D), 2012). Continued work with the model has shown that wave action drives the particles from the seabed to the Dounreay foreshore where the bulk of particles are found. Reviews of potential new or ongoing sources of particles have been conducted and do not find evidence of either case, leading to the conclusion that all particles found are from past releases (Dennis et al., 2007). The majority of the particles from Dounreay are attributed to the reprocessing of fuel from either the MTR or the DFR. However, a few particles with other characteristics have been identified, including ^{60}Co containing particles and ^{90}Sr enriched particles with activities of ^{90}Sr significantly greater than for ^{137}Cs (PRAG(D), 2012).

Estimates suggest there are several hundred thousand Dounreay particles in the surrounding environment although the risk to members of the public remains very low (Dale et al., 2008; Henderson et al., 2007; Tyler et al., 2010). In conjunction with Dounreay Site Restoration Ltd. (DSRL), routine monitoring of affected areas using vehicle mounted detectors was established and the number of particle finds increased to an average of eight per month (PRAG(D), 2012). The detection limit and efficiency of doing so would depend not only on the detector, but also on the speed of the vehicle. Complete inventories of particle finds are available to the public through DSRL (DSRL, 2019a; DSRL, 2019b; DSRL, 2019c). The radioactivity of particles largely depends on the size and typically varies from 10^2 to 10^7 Bq, MTR particles having significantly higher activities than the ones originating from DFR operations. To develop a categorization of the particles based on activity, and thereby health risk, SEPA organizes recovered particles by ^{137}Cs activity, which is easy for recovery teams to measure by gamma spectrometry (PRAG (D), 2012). The ^{137}Cs activity particles with the highest activities, i.e., above 10^6 Bq, are termed *significant*. *Relevant* particles contain $>10^5$ Bq ^{137}Cs, while any particle with ^{137}Cs activity below 10^5 Bq is classified as *minor*. The majority of particles identified fall into the *minor* classification. As the size distribution of radioactive particles found at other contaminated sites would, to a certain extent, follow a log-normal distribution (Kashparov et al., 2000; Shevchenko, 2004), the potential exists that a significant number of undetected, low activity particles would be situated in the marine ecosystem and the beaches around the Dounreay facility, and that the *minor* classification category could be defined too broadly.

Radioactive particles, like Dounreay fuel fragments, can carry a substantial amount of radioactivity and act as point sources of potential long-term significance for human health as well as for biota (Salbu et al., 2018). There is a risk from inhalation, dermal absorption, skin exposure, and ingestion. For filter-feeders (e.g., mollusks) and soil-dwelling animals (e.g. gastropods), particles can be retained by the organism and eventually be ingested by humans (Jaeschke et al., 2015; Salbu et al., 2018). Upon prolonged contact, radioactive particles can give rise to skin ulceration (Charles, 1991; Darley et al., 2003; Gesell et al., 1999) and damage epithelial tissues of biota (Jaeschke et al., 2015). Furthermore, particle weathering can increase the mobility and potential for the transfer of particle associated radionuclides into the biosphere. As a result of particle weathering, radionuclides originally associated with large particles or fragments may also occur as submicron and even nanoscale particles with biological uptake properties potentially very different from those of ions (Salbu et al., 2018). Thus, uncertainties in environmental impact assessments of particle contaminated areas may be unacceptably large if heterogeneous distributions are not taken into account. At Dounreay, uncertainties are magnified by the potential existence of small, non-detected particles in the marine environment. Previous risk assessments related to Dounreay particles have primarily focused on human health. However, environmental biota are not necessarily adequately protected from ionizing radiation even if humans are sufficiently protected (Strand et al., 2009).

The purpose of the present work is to fill identified knowledge gaps associated with Dounreay fuel fragment characteristics by linking data on morphology, elemental and isotopic composition, as well as oxidation state to the release scenario and potential health risks. To achieve these goals, the present work presents (1) new information on Dounreay fuel fragment characteristics based on analysis using laboratory based X-ray fluorescence (μ-XRF), scanning electron microscopy (SEM-XRMA), and inductively coupled plasma mass spectroscopy (ICP-MS), (2) results from synchrotron radiation based micro X-ray Absorption Near Edge Spectroscopy (μ-XANES), and (3) an estimation of the potential contact dose from encountering a particle by direct beta measurements using a Si semiconductor detector (Canberra PIPS) and skin dose calculator software VARSKIN6.

2. Materials and methods

2.1. Particle handling and gamma spectrometry

Archived particles (3 of the DFR type and 3 of the MTR type) were supplied from SEPA for analysis. The original particle details are shown in Table S1. Some of the particles were utilized in connection with previous blue mussel exposure experiments in which physical deterioration and loss of activity from particles were observed in some cases (Jaeschke et al., 2015).

Individual particles were re-examined by gamma spectrometry using a liquid nitrogen cooled Low Energy Germanium (LEGe) detector (Canberra Instruments, relative efficiency 25%, resolution 1.8 keV) with particles being counted at 10 cm distance from the surface of the detector. SEM-XRMA and μ-XANES measurements were completed prior to exposure experiments with blue mussels (Jaeschke et al., 2015). All μ-XRF and dosimetry measurements were completed after the blue mussel studies.

2.2. ICP-MS

Small fragments of DFR3 and MTR2 were sacrificed for ICP-MS analysis in order to determine the isotope ratio $^{235}U/^{238}U$ as well as niobium (Nb), molybdenum (Mo), neodymium (Nd), and zirconium (Zr) concentrations. The samples were isolated from the main particle and dissolved by microwave digestion (Milestone, Ultraclave III, Italy) at 260 °C for 40 min in a 1 mL mixture of HNO_3, H_2PO_4, and HBF_4 (1:2:1 ratio). An acid mixture selection was made to ensure proper dissolution of Nd along with other metals. The isotope ratios and element concentration were determined by inductively coupled plasma mass spectrometry (Agilent 8800 ICP-MS QQQ, Japan). Isotopic ratio results were mass bias corrected against a 6 μg/L solution of NBL CRM 129-A isotopic standard.

2.3. SEM-XRMA

Individual radioactive particles or sub-samples from these (~10–50 μm grains extracted with tweezers) were attached to carbon double-faced sticky tape and mounted onto Al stubs for analysis of surface structures and elemental composition of the particles by means of scanning electron microscopy (SEM) using a JEOL JSM 840 instrument interfaced with an ISIS 300 X-ray micro-analysis (XRMA) system, Oxford Instruments. Surface structures were viewed using secondary electron imaging (SEI) mode, while backscatter electron imaging (BEI) mode highlighted high density (high atomic number elements) areas as bright structures on the image. XRMA provided semi-quantitative identification of elements. The distribution of elements were shown by x-ray mapping helping to identify locations containing U and other elements of interest (Salbu and Lind, 2020).

2.4. Laboratory based μ-XRF

Each of the particles, or fragments of the original particle, were subjected to laboratory based micro X-ray fluorescence (μ-XRF) to determine the elemental distribution on the particle surface and isotope ratios using a M4 Tornado (Bruker, Germany) (Janssens et al., 2010). Particles were remounted from the SEM stub to a mylar foil stretched over an x-cell (31 mm Double Open-Ended X-CELL®). A rhodium (Rh) target, running at 50 kV and 600 μA, and polycapillary optics provided the beam with a spot size of 25 μm. Fluorescent x-rays were counted by two XFlash® silicon drift detectors (50 keV, 600 μA, 25 μm spot size). The detectors are at a 45° angle to the beam and each feature an active area of 30 mm^2. Two-dimensional elemental mapping was performed under vacuum (20 mbar) and repeated a number of times to ensure good statistics. Collected XRF spectra were analyzed by the ESPIRIT software (Bruker).

2.5. Synchrotron based μ-XANES

After SEM-XRMA analysis, sub-samples from particles DFR2 and MTR3, mounted on carbon double-faced sticky tape, were examined by synchrotron based micro X-ray absorption near edge spectrometry (μ-XANES) analysis using the x-ray microscopic facility at beamline L, HASYLAB, Hamburg (Lind et al., 2007; Lind et al., 2009; Salbu et al., 2003). By tuning the monochromatic, focused x-ray beam (20 μm beam via polycarpellary lens) over the U L_{III} absorption edge (17.163 keV), information related to the oxidation state of U present in the particles can be found (Conradson et al., 2004; Salbu et al., 2001; Schulze and Bertsch, 1995; Silva and Nitsche, 2001). The beam flux at the sample spot was approximately 10^9 photons per second at 17.1 keV. The beam intensity was measured by ionization chambers and the U L_{III} fluorescence intensity was measured by a well collimated, high purity germanium (HPGe) detector (area of 30 mm^2) mounted at a 90° angle to the primary beam and 30 mm from the sample. The μ-XANES spectra were collected over 300 eV in 1 eV increments. Well defined U oxidation standards (UO_2, Institute of Energy Technology, Kjeller; U_3O_8, Institute of Energy Technology, Kjeller; UO_2Ac_2 x $2H_2O$ p.a., Riedel-De Haën AG, Seelze-Hannover; $UO_2(NO_3)_2$ x $6H_2O$ p.a., Merck, Darmstadt) were used to collect standard μ-XANES spectra for comparison with sample spectra.

2.6. Contact dosimetry

Beta ray emissions from individual radioactive particles were determined using a SPAB15 alpha/beta probe connected to a Radiagem 2000 Portable Dose Rate and Survey Meter (Canberra). The particles were counted for 30 s at 1 cm increments to a minimum of 20 cm. The observed count rates were corrected for detector efficiency: 37% for $^{90}Sr/^{90}Y$ (Menanteau, 2009). The beta activity for each particle was calculated using the relationship between the corrected count rate and the particle activity (Bq) in Eq. (1) (Choppin et al., 2013).

$$\text{Corrected Count Rate cps} = \psi_{sample}\psi_{abs}\psi_{geom} \times \text{Particle Activity Bq} \quad (1)$$

here, ψ_{sample} represents the self-absorption of beta rays within the particle. Because the particles are small (<2 mm), ψ_{sample} is taken to be 1. Air attenuation is accounted for by ψ_{abs} and the geometric correction is denoted by ψ_{geom}.

VARSKIN6, a skin dosimetry calculator developed by the United States Nuclear Regulatory Agency (USNRC), was used to compare skin dose estimates provided by Harrison et al., 2005. (Gesell et al., 1999). Combined β-γ skin dose estimates were made for contact doses of a 1 cm^2 area to the epithelial layer of skin (70 μm below the surface) with no mediating shield (Anspach and Hamby, 2018).

3. Results and discussion

The DFR particles examined in this study are classified as *minor* particles by SEPA, while the MTR particles belong to the *relevant* category. DFR particles were below 300 μm in size and appear non-metallic, brittle, and prone to mechanical breakdown, which is important with respect to particle weathering as the surface area of the original particle increases after breaking. Estimates of the specific gravity of DFR particles suggest a broad range of 4.7–7.4 g/cm^3 (Dennis et al., 2007). The MTR particles studied here were larger (<2 mm in size), mostly of metallic appearance and sturdier (Table 1). According to SEPA, the MTR particles in general range from 0.4 mm to 3 mm in size and have a density of 3.1 ± 0.4 g/cm^3 (PRAG(D), 2012).

3.1. Characteristics of DFR particles

Scanning electron microscope imaging of the DFR type particles detail surfaces that are pitted and cracked, giving credence to the assumption that DFR particles lack structural stability (Fig. 2), in line with previous descriptions (Henderson et al., 2007; Potter et al., 2003). Of note, the surface morphology of DFR2 varies across the particle with predominately pitted, porous material along with a few crystallized, smoother regions, indicating a variation in the formation of the original particle or its subsequent weathering. X-ray microanalysis at various locations on the particle surface show the dominant elements to be U and Nb with some inclusions of iron (Fe).

According to the PRAG(D) report (PRAG(D), 2012), DFR particles are expected to contain approximately 40% Nb, 20% U, and 15% Fe. X-ray point analysis on the pitted, porous regions also found titanium (Ti), sodium (Na), aluminum (Al) and Zr to be present. In a nuclear context, Zr is typically related to the cladding material of fuel elements, although Zr can also occur naturally in soils and sediments. In addition, a wide range of elements indicative of soils or sediments adhering to the particle surfaces were identified, such as chlorine (Cl), sulfur (S), and phosphorus (P).

Table 1
Characteristics of particles analyzed in this work (reference date: October 2018).

Particle	Approximate particle dimensions (μm)	$^{235}U/^{238}U$ isotope ratio	Major elements	Elemental ratios mean ± σ (range)	Number of point measurements	^{137}Cs activity (Bq ± σ)
DFR1	100 × 90	N.A.	U, Nb, Mo, Fe, Cr, Al, Ni, Si, Zn	Nb/U = 2.4 ± 0.3 (2.1–2.9) Mo/U = 0.02 ± 0.02 (0–0.1)	8	(2.0 ± 0.1) × 10^3
DFR2	200 × 160	N.A.	U, Nb, Mo, Fe, Cr, Al, Si, Zn	Nb/U = 2.5 ± 0.3 (1.9–3.0) Mo/U = 0.02 ± 0.01 (0–0.03)	10	(6.9 ± 0.2) × 10^3
DFR3P1	300 × 160	3.2 ± 0.8	U, Nb, Mo, Fe, Ca, Cl	Nb/U = 2.1 ± 0.1 (1.9–2.2) Mo/U = 0.1 ± 0.02 (0.03–0.1)	4	(6.6 ± 0.2) × 10^3
DFR3P2	300 × 160	3.2 ± 0.8	U, Nb, Fe, Zn	Nb/U = 2.1 ± 0.1 (1.9–2.2) Mo/U = 0.1 ± 0.02 (0.03–0.1)	4	(9.6 ± 0.3) × 10^3
MTR1	2000 × 1000	N.A.	U, Al, Nd, Fe, Zn, Si	Al/U = 19.8 ± 5.7 (9.5–33.6) Nd/U = 0.02 ± 0.003 (0.01–0.03)	100	(6.4 ± 0.1) × 10^5
MTR2	1400 × 300	2.6 ± 0.4	U, Al, Nd, Zn, Mg, Fe	Al/U = 14.6 ± 8.0 (4.2–56.6) Nd/U = 0.1 ± 0.03 (0.03–0.3)	100	(4.3 ± 0.1) × 10^4
MTR3	50 × 30	N.A:	U, Al, Si, Fe, Ca, Ni, Cr	Al/U = 378 ± 242 (35.5–551) Nd/U = 0.5 ± 0.2 (0.3–0.7)	3	(3.7 ± 0.3) × 10^2

N.A. = not analyzed.

Both SEM-XRMA and μ-XRF analyses show a correlation between U and Nb (Fig. 2, Fig. 3, Fig. 4) and the elemental ratio between Nb/U was approximately 2 for all DFR particles (Table 1). Elemental mapping by μ-XRF also shows a spatial correlation between Nb and U. To further test the Nb-U correlation, a sub-sample of DFR3 was analyzed via ICP-MS and found a Nb/U ratio of 1.7 ± 0.2, in good agreement with the μ-XRF results.

The same ICP-MS results yielded a $^{235}U/^{238}U$ ratio of 3.2 ± 0.8 for DFR3, showing that the U present in the particle was highly enriched (HEU) according to the IAEA classification (IAEA, 2005). The fuel elements used in the DFR were highly enriched U-Mo slugs, clad in a Nb casing (Cartwright, 1997). Investigations by SEPA indicate that the DFR particles were formed by high temperature (1668 °C) dissolver accidents during fuel element dissolution (Henderson et al., 2007). Such high temperatures would exceed the temperature threshold to form a U and Nb alloy such as UNb_2O_7 (Busch and Gruehn, 1994). The formation of such an alloy was supported by x-ray analysis of the DFR particles. The U-L_{III} edge μ-XANES spectra in a subsample of particle DFR2 coincide with the spectrum for UO_2 (Fig. 5) and strongly indicates that U is tetravalent, i.e., present as UO_2 or as an intermetallic compound. The latter interpretation is arguably supported by SEM-XRMA analyses, which showed U and Nb

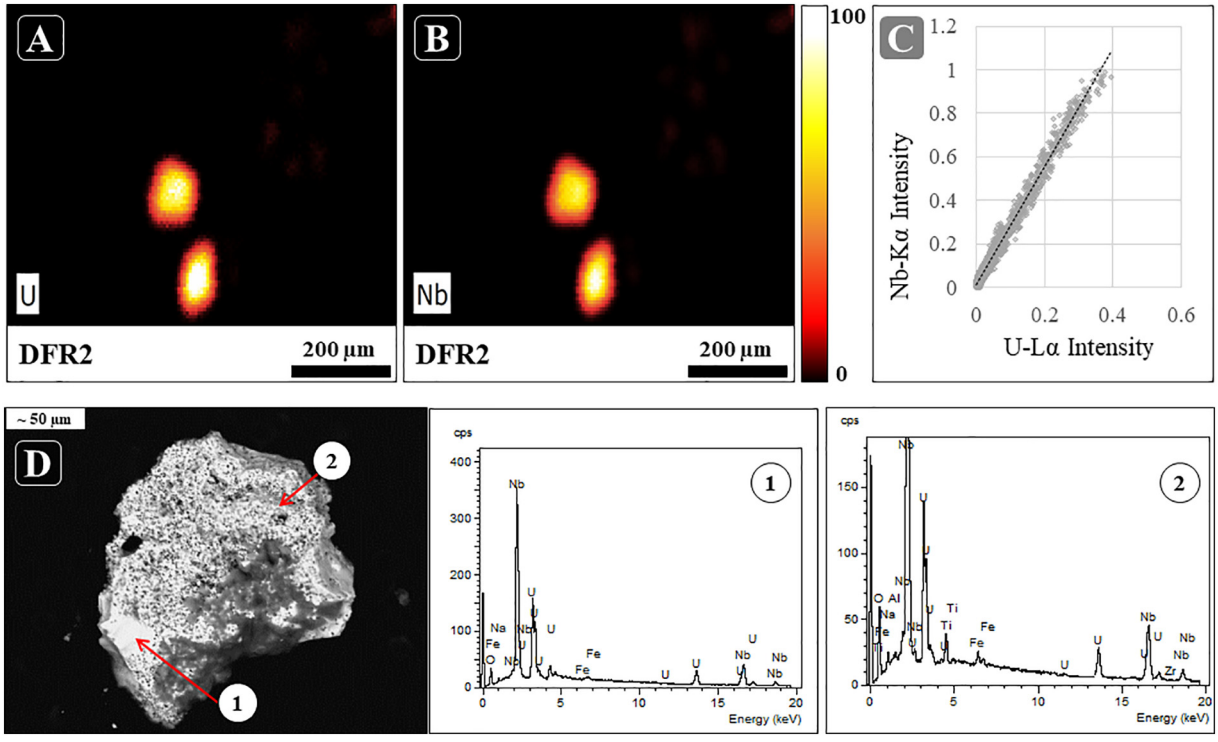

Fig. 2. Elemental mapping by μ-XRF of DFR2 showing (A) the U and (B) the Nb distributions (intensity scale on the right). C) Correlation plot of normalized U Lα and Nb Kα intensities from the XRF elemental mapping. D) SEM BEI image with XRMA spot analysis at a flat smooth region at location (1) and at a porous, pitted region at location (2).

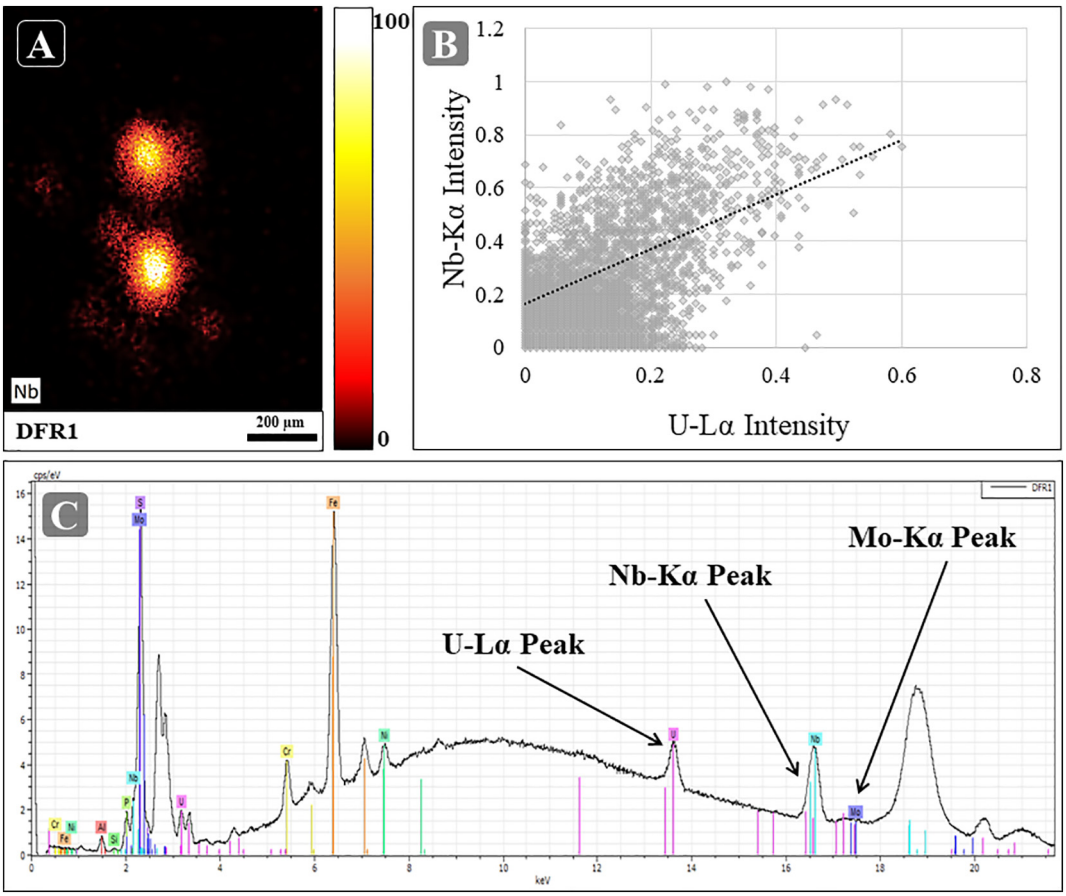

Fig. 3. (A) Nb map of DFR1 obtained by micro-XRF. (B) Correlation plot between normalized U Lα and Nb Kα intensities obtained in (A). (C) XRF spectrum collected from DFR1, showing the U, Nb, and Mo peaks.

co-existing at the micron scale resolution throughout the particle matrices and by Nb/U atom ratios of ~2 observed in μ-XRF analyses. These stoichiometric considerations are commensurable with the presence of UNb_2O_7 in the particles.

Leaching experiments have previously been conducted to investigate the potential bioavailability of DFR particles using simulated human stomach juices (2 h) and two types of intestinal fluids (2 × 4 h), sequentially (Stewart et al., 2003). Results show that, on

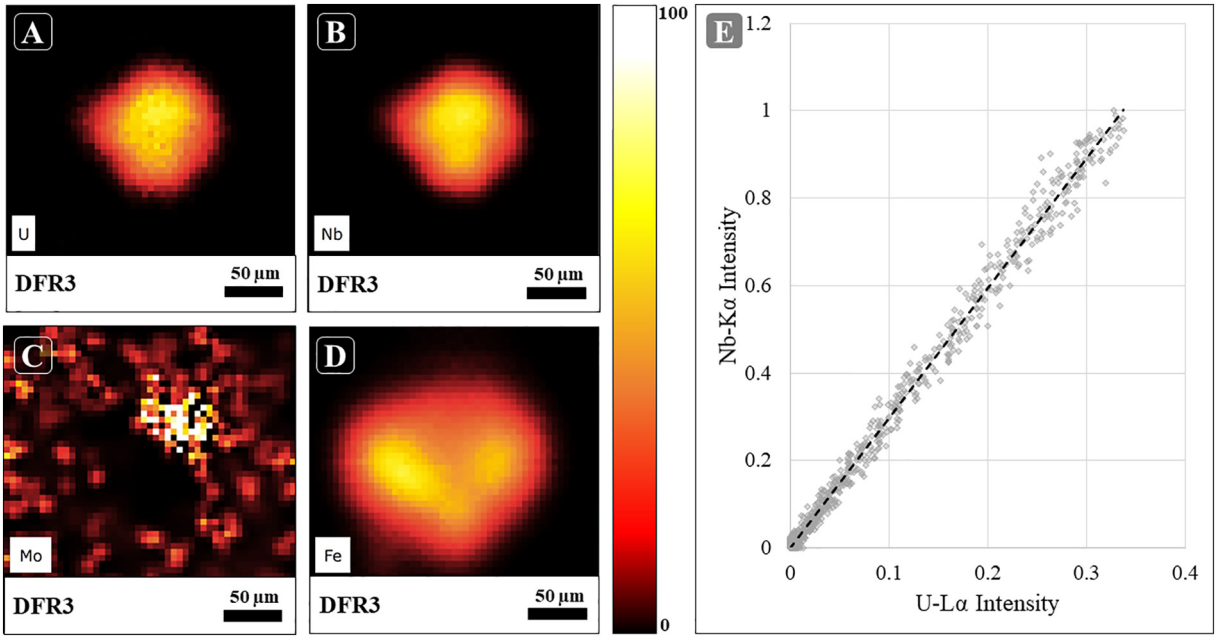

Fig. 4. Micro-XRF elemental maps of DFR3:(A) U, (B) Nb, (C) Mo, and (D) Fe distributions. (E) Correlation plot of normalized intensity signals of U-L_α and Nb-K_α obtained in (A) and (B).

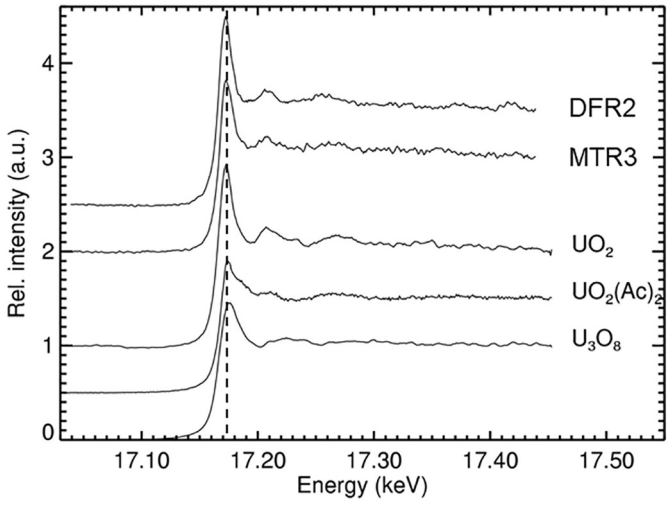

Fig. 5. Fluorescent U μ-XANES profiles obtained from fragments of Dounreay particles DFR2 and MTR3 in comparison to UO_2, $UO_2(Ac)_2$ and U_3O_8 reference compounds. Vertical line indicates position of white line of UO_2.

average, 47% of ^{137}Cs and 85% of ^{241}Am were removed from DFR particles. These results can provide insight into the general mobility and bioavailability of radionuclides associated with these particles and suggest a significant mobilization potential. However, a study of retention of DFR particles in rats found only 1% retention in most cases for the major radionuclides of interest, giving credence to the assumptions that DFR particles do not readily dissolve in the body prior to excretion (Harrison et al., 2005). This conclusion is supported by the fact that the DFR particles have resided approximately 40–50 years in the marine environment, yet, have retained significant concentrations of U and fission products. Given the range of results from these studies, leaching experiments could provide a fertile ground for future work with these particles.

In addition to U and Nb, trace amounts of Mo were detected in each DFR particle (Table 1). Molybdenum was correlated with U, commensurate with the fact that the DFR nuclear fuel contained Mo, which was used to improve thermal stability during irradiation of the fuel element (Cartwright, 1997; Meyer et al., 2014; Rest et al., 2006). In DFR3, the elemental mapping of Mo was possible and showed spatial correlation with U and Nb (Fig. 4). Although it is claimed that DFR fuel contained an approximate atomic concentration of 15% Mo (Meyer et al., 2014), our μ-XRF analyses suggest that Mo is only present in atomic concentrations of ~1%. The Mo loss can possibly be attributed to oxidation and removal of Mo from the fuel as MoO_3 during the high temperature formation of the particles. Material testing of U-Mo type fuels have shown that the significant porosity in fuel elements was similar to the porous, pitted surfaces observed in the present DFR particles, and this could be attributed to the formation of so-called high burnup structures (Jadernas et al., 2018; Leenaers et al., 2016).

3.2. Characteristics of MTR particles

The examination of MTR type particles displayed the rigid crystalline and metallic appearance described in previous reporting, as illustrated in Fig. 6 for particle MTR3. Scanning electron microscopy in BEI mode combined with spot XRMA analysis of the three studied MTR samples show that the particle surfaces contain a matrix of Al and U distributed inhomogeneously. Particle surface elements also included Na, Ca, Si, P, S, and, most significantly, Fe. These elements are common amongst

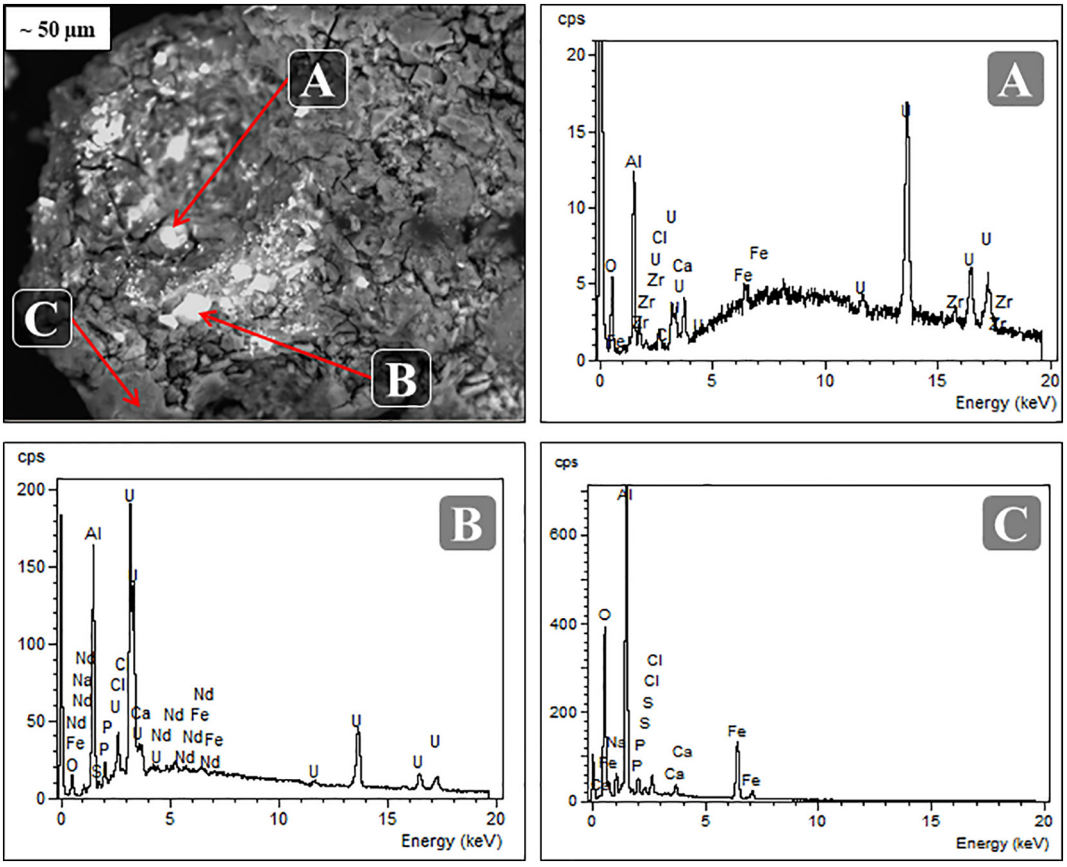

Fig. 6. SEM-XRMA of MTR3. High density regions appear as bright locations on the surface of the particle. SEM-XRMA spectra from three MTR3 locations (A), (B), and (C). High density locations (A) and (B) contain U, while darker location (C) appears to mostly contain Al.

marine sediments and it is plausible that they fill cracks and pores on the particle surfaces due to environmental processes (Potter et al., 2003)

Notably, Nd is present throughout U containing phases of the particle reaching 1–2% by mass, suggesting Nd was included in the original fuel design (Potter et al., 2003), rather than present due to decay of fission products as suggested elsewhere. The X-ray microanalysis of MTR3 also yielded signals of Nd on the surface of the particle that generally were spatially correlated with the U distribution (Fig. 6B). Using μ-XRF elemental mapping, the MTR particles show an inhomogeneous distribution of elements throughout, as seen in Figs. 7 and 8, making each one somewhat unique.

The MTR was fueled by a U dispersion fuel that comprised of small grains, a few microns in size, of uranium-aluminum (UAl_4) embedded in an Al substrate and housed in an Al casing (Gibson, 1997; Tamborini, 2004). Together, the components formed a flat, panel shaped fuel element approximately 2 mm in thickness that includes both the UAl_4 core and the Al casing (Henderson et al., 2007). The fuel elements contained approximately 20% U by weight and had an average enrichment of 70% ^{235}U, with some assemblies containing as high as 90% enrichment (Henderson et al., 2007; Potter et al., 2003). Grinding and cutting operations on the MTR fuel plates were conducted as part of the fuel reprocessing, designed to remove excess Al, but occasionally cut too close to the U containing core and generated swarf that included fuel fragments (DPAG, 2008). In the particles studied, Al was inhomogeneously distributed across each particle with noted enriched areas. Multiple spot μ-XRF analyses on the surface of particle MTR1 revealed a wide variation in Al/U ratios (Fig. 7). Smooth, shiny locations with a metallic luster on the surface exhibited an Al/U atomic ratio of ~16, while the corresponding ratio measured at a dark pit on the surface was significantly lower (~10). The inhomogeneous distribution of Al is likely representative of both the design of the MTR fuel matrix as well as potential mechanical fragmentation from exposure to the environment, as evidenced by the dark pits on the surface of the particle. Analyses made here would indicate that the local U concentration is, on average, 25–45% by weight depending on the location within the particle. Thus, assumptions about the average density of MTR type particles may be affected with large uncertainties.

Secondary ion mass spectrometry (SIMS) of a MTR particle has previously showed the distribution of micron scale inclusions of enriched U within the Al matrix (Tamborini, 2004). An overall Al/U atomic ratio of 6.9 was determined by SIMS and ICP-MS for the examined particles. The resolution of the SIMS instrument (~1 μm) allowed for measurement on the UAl_4 grains themselves while the μ-XRF in this study had a beam size of 20 μm and would collect signal from the surrounding Al material. The isotopic composition (83% ^{235}U, 8% ^{236}U, 8% ^{238}U by atomic concentration, $^{235}U/^{238}U = 10$, $^{239}Pu/^{240}Pu = 6.0$) of the MTR particle in that study was consistent with a calculated composition of HEU fuel with an enrichment of >90% that had been irradiated in an MTR reactor to a burnup of 25–30% (Tamborini, 2004). Results from the present ICP-MS analysis of a fragment from MTR2 showed a slightly lower, but still HEU, $^{235}U/^{238}U$ isotope ratio of 2.6 ± 0.4. However, this variation can be attributed to the original fuel assembly the particle was derived from, as not all fuel assemblies had the same enrichments or burn-ups.

Given that the original MTR fuel was an alloy of Al and the intermetallic compound UAl_4, the U containing phases in MTR particles may remain UAl_4, especially as the assumed formation and release pathway of the particles involved grinding and cutting, but not high heat dissolution (Potter et al., 2001). Examinations of UAl_4 have found that it is well formed with few defects in the structure of the U sublattice, suggesting that the compound is quite sturdy and that fission products are well bound to the structure, important to the potential leaching (Potter et al., 2001; Tougait and Noel, 2004). However, there remains the potential for oxidation of the surface of the particle. Research into the corrosion of uranium aluminide fuels, when placed in long term storage under aqueous conditions, identified oxidation on the surface of the fuel elements that included a UO_2 phase (Kaminski, 2003; Kaminski and Goldberg, 2002). The occurrence of UO_2 in those fuel assemblies was part of a process that resulted in the formation of schoepite on U containing surfaces. The μ-XANES analysis (Fig. 5) of a subsample of MTR3 most closely related to those of the UO_2 standard, indicating the U could be present as U(IV). Although qualitative, U in

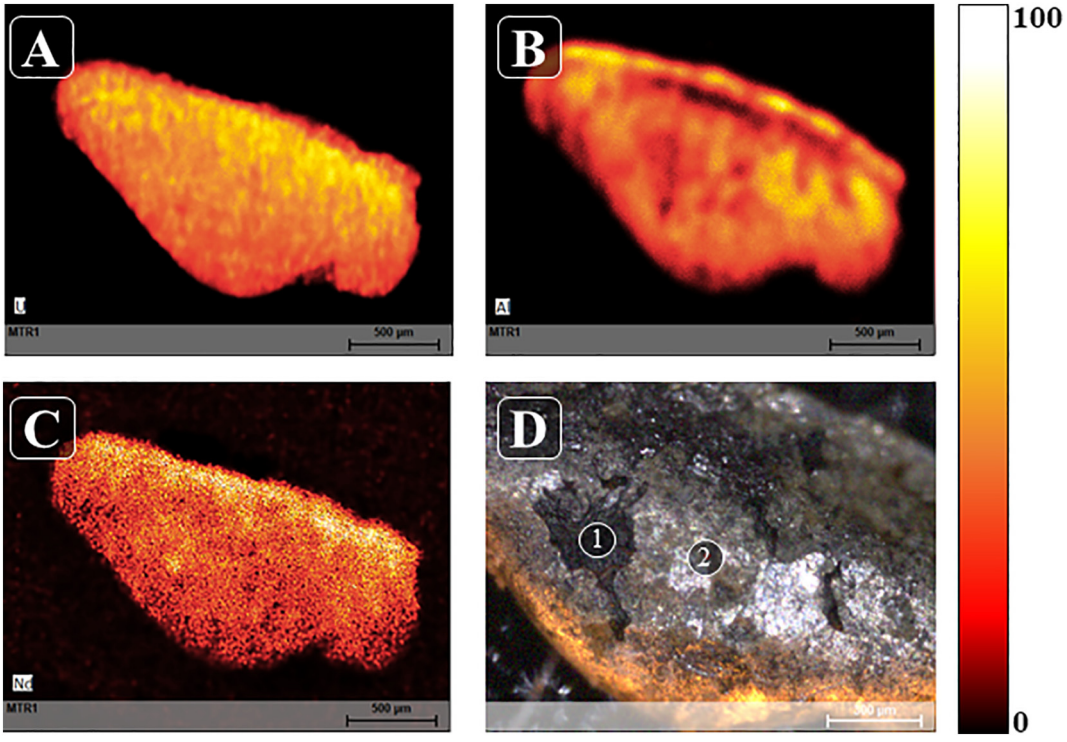

Fig. 7. Elemental maps obtained by μ-XRF: (A) U, (B) Al and (C) Nd distributions within particle MTR1. (D) Light micrographs of the surface of MTR1 show the locations of point measurements (1) and (2), featuring a change in Al/U ratio: 9.6 at (1) and 15.8 at (2).

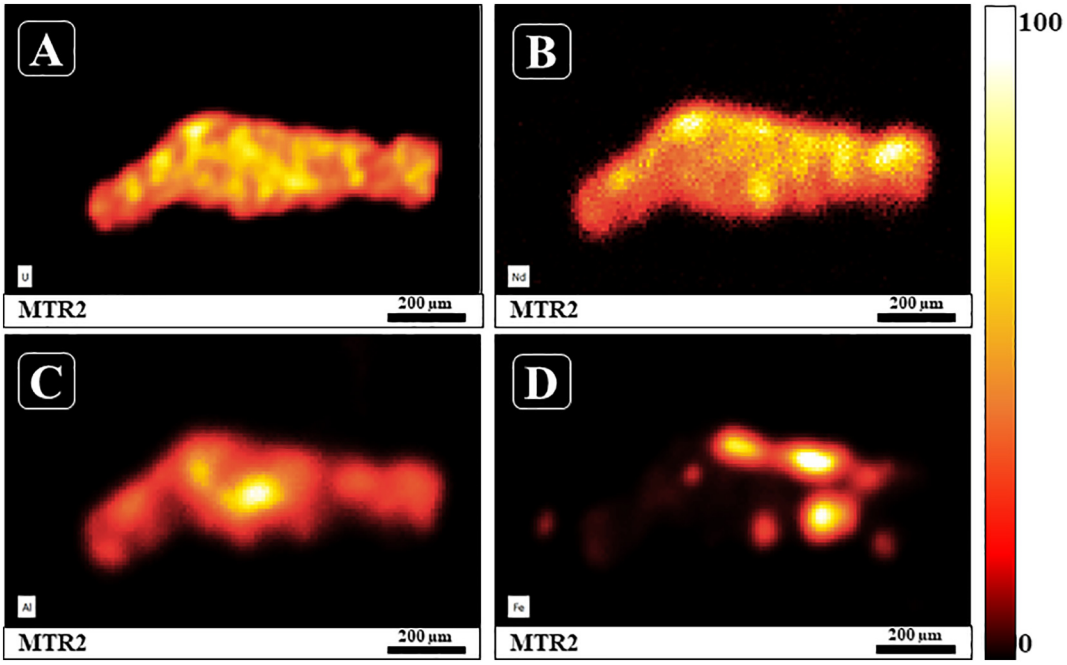

Fig. 8. Micro-XRF elemental maps of (A) U, (B) Nd, (C) Al and (D) Fe in MTR2, showing the inhomogeneous distribution of elements. The intensity scale bar indicates atomic concentration (in %) of the element shown.

the U(IV) state suggest that the exposed U containing phases on the surface of the MTR particle are oxidized. In addition, Kaminski et al. have shown U colloid formations from the corrosion of the fuels to be significant (Kaminski et al., 2005). These studies show that UO_2 is plausible as an intermediate phase in the corrosion of UAl_x type fuels that the MTR particles are derived from and that the potential exists for the formation of U containing colloids during weathering of the particles. The weathering of particles has been shown to decrease the overall particle size distribution giving rise to a colloidal phase and similar responses could be expected for MTR particles (Salbu et al., 2018). However, the analysis via μ-XANES in this study is only qualitative and represents a small subsample of only one particle and further investigation of U in MTR particles is required to confirm these results, such as Extended X-ray Absorption Fine Structure (EXAFS) analysis.

Stewart and coworkers conducted leaching experiments with MTR particles in the same way as for DFR particles (Stewart et al., 2003). The study showed similarly high leaching rates of particle associated radionuclides (60% ^{137}Cs, 51% ^{241}Am) as for DFR particles, suggesting a rather high remobilization of these radionuclides from the fuel matrix. This leaching behavior, along with the potential for colloid formation such as reported by Kaminski et al. (2005), indicates that these particles may be prone to rapid weathering. Thus, the use of the IAEA CRP/EU COMET-RATE protocol for abiotic leaching, including size fractionation of leachates (Salbu and Lind, 2020), should be scope for further studies on Dounreay particles.

3.3. Contact dosimetry from Dounreay particles

An assessment of the activity and contact dose rates of the six particles was made and compared with published, generalized estimates (Harrison et al., 2005). Based on gamma spectrometry, ^{137}Cs activities ranged from 2.0×10^3–9.6×10^3 Bq/particle for DFR particles and 4.3×10^4–6.5×10^5 Bq/particle for MTR particles (Table 2). Due to the high concentration of ^{90}Sr in Dounreay fuel fragments, beta doses from contact with a particle pose a significant risk. Based on the SPAB15 probe measurements, beta activities ranged from 1.6×10^3–7.3×10^3 Bq/particle for DFR particles and 3.5×10^4–5.3×10^5 Bq/particle for MTR samples (Table 2). As expected, beta activities were slightly lower than ^{137}Cs activities and the calculated beta/^{137}Cs ratio was approximately 0.8 for all the studied particles except DFR3P1 which showed a ratio of 0.9. The measured beta activities were lower on average than the estimates made by SEPA, which relies on a ^{90}Sr/^{137}Cs ratio of 0.9, shown in Fig. 9 (Aydarous et al., 2008; Aydarous et al., 2001; Harrison et al., 2005).

SEPA estimates the ^{90}Sr activity in a MTR type particle to be 0.9 of the ^{137}Cs activity, based on isotopic composition analyses (Darley et al., 2003; Harrison et al., 2005; Wilkins et al., 1998). Because they are found in higher abundance, have higher activity, and are of sturdier nature than DFR particles, only MTR particles were assessed by SEPA. As a result, the evaluation states that it will overestimate doses for DFR particles. The results shown here indicate that the 0.9 ratio only slightly

Table 2
Activity and dosimetry results for DFR and MTR particles examined in this paper.

	^{137}Cs activity via HPGe (Bq)	Beta activity via SPAB 15 measurements (Bq)	Beta activity/^{137}Cs activity	VARSKIN6 skin dose rate (mGy/h)	Time to 500 mGy threshold[a] (hrs)
DFR1	$(2.00 \pm 0.09) \times 10^3$	$(1.61 \pm 0.08) \times 10^3$	0.81	0.22	2273
DFR2	$(6.94 \pm 0.19) \times 10^3$	$(5.75 \pm 0.29) \times 10^3$	0.83	0.79	633
DFR3P1	$(6.55 \pm 0.20) \times 10^3$	$(5.91 \pm 0.30) \times 10^3$	0.90	0.82	610
DFR3P2	$(9.58 \pm 0.27) \times 10^3$	$(7.95 \pm 0.40) \times 10^3$	0.83	1.3	385
MTR1	$(6.41 \pm 0.10) \times 10^5$	$(5.30 \pm 0.27) \times 10^5$	0.83	74	7
MTR2	$(4.32 \pm 0.09) \times 10^4$	$(3.53 \pm 0.18) \times 10^4$	0.82	4.9	102
MTR3	$(3.73 \pm 0.30) \times 10^2$	$(3.02 \pm 0.15) \times 10^2$	0.81	0.04	12,500

[a] NCRP 130

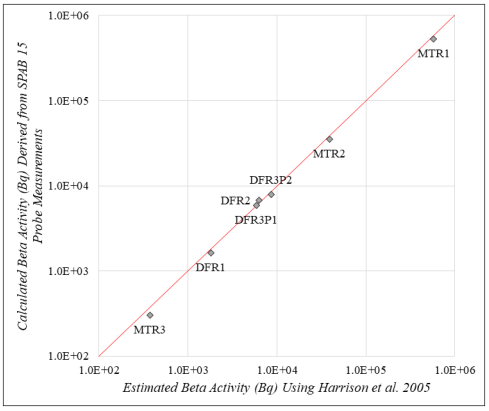

Fig. 9. Correlation between the beta activity (in Bq) determined by the SPAB 15 probe measurements (vertical) and the beta activity estimated according to the method by Harrison et al. (2005) (horizontal). The red diagonal indicates a 1:1 comparison of estimated beta activity based on gamma spectrometry versus calculated beta activity based on direct beta measurements. Particles above the red line have larger estimated activity values, based on gamma activities; particles below the red line have larger estimated activity values based on direct beta measurements.

(i.e., maximum 10%) overestimates the beta activity for all studied particles except for the fragment of DFR3P1.

VARSKIN6, a computer code from the USNRC (Anspach and Hamby, 2018), was used to perform contact dose rate calculations based on the activity determined by gamma spectrometry and from the SPAB15 measurements. VARSKIN6 estimates doses and dose rates based on an assumed infinitely small point source on the surface of the skin. In contrast, the estimate made in Aydarous et al., 2008 was employing Monte Carlo calculations based on radiochromic dye film exposures of MTR type particles. The Monte Carlo estimations were made assuming a homogeneous MTR particle of 15% U composition, an average density of 3.1 g/cm^3, and accounting for variation in particle shape and self-absorption. For particles with a ^{137}Cs activity of 10^4 or 10^5 Bq, the assessment by SEPA outlines expected contact skin dose rates of 30 or 300 mGy/h, respectively. For direct comparison, the MTR1 and MTR2 particles would fit to the same assessments, and the VARSKIN6 calculated dose rates were 74 and 4.9 mGy/h, respectively (Table 2). Although these estimates will suffer from uncertainties, the VARSKIN6 code does not provide for uncertainties on the calculated results. The National Council on Radiation Protection and Measurements (NCRP) outlines an occupational health threshold for radioactive particle skin dose of 0.5 Gy (Gesell et al., 1999). The particles assessed in this study would require contact times of several hundred hours to reach this threshold, with the exception of the large MTR particles, particularly MTR1, which would deposit 0.5 Gy in 7 h (Table 2).

Risk assessments associated with Dounreay particles have been based on assumed low probabilities of man and organisms encountering highly radioactive (*significant*) particles in the environment (Jackson et al., 2007; Pellet, 2004; Smith and Bedwell, 2005). However, both field observations (on gastropods) and laboratory experiments (on filter feeders) have shown that ingestion and retention of particles does occur and that retained particles may induce acute effects (Jaeschke et al., 2015). The dose assessment in this report is lower than the TLD based assessment made in Jaeschke et al. and the difference should be attributed to the dose assessment method used. Given that the retention times for particles retained in blue mussels were high (70 h), the threshold to skin ulceration, 2 Gy (NRPB, 1997) would be reached using both assessment methodologies.

Radioactive particles, including those originating from Dounreay, will be subject to weathering, transforming larger fragments to small, bioavailable species, of relevance for biological uptake, retention, and subsequent dose impact, as well as risk assessments for particle contaminated sites (Shevchenko, 2004). The bioavailability and uptake of particle-bound radionuclides compared with those existing as ions or simple molecules has so far largely been ignored when impact and risks are assessed (Salbu, 2016). As a result, there is a high degree of scientific uncertainty about the long term ecological consequences and risk to human health from radioactive particles present in the environment (IAEA, 2011). Finally, these factors contribute to the overall challenge related to conceptual or structural uncertainties in environmental impact and risk assessments associated with radioactive particle contaminated areas (Salbu, 2016). Important aspects of the contamination are often ignored, such as source term and particle characteristics with implications for transport, deposition, and ecosystem transfer. In addition, particle specific weathering and dynamics can change uptake pathways and retention in organisms resulting in particle specific dose estimates that are unevenly distributed. These structural challenges are present in dose assessments for Dounreay particles, but the results presented in this work should contribute to reduce the uncertainties.

4. Conclusions

Two types of Dounreay U fuel particles, DFR and MTR, were characterized with respect to particle structure and morphology, elemental and U isotopic composition, as well as oxidation states of U via techniques not previously employed (μ-XRF and μ-XANES). The results provide clues about the speciation of U in the particles and can be linked to source term and release scenarios. The studied DFR particles appeared to contain UNb_2O_7 formed during fuel dissolution, while the MTR particles appeared to contain UAl_4 + Al, as stated in the fuel design. The μ-XANES data suggest that particle weathering and oxidation of particles surfaces have to a certain extent occurred.

Previously unreported elements, Mo (<1%) in DFR particles and Nd (1–2%) in MTR particles, were identified. As previous characterization of Dounreay particles only considered an average MTR particle of uniform composition, the structural and elemental analysis presented here should prove useful for developing a representative DFR particle model as well as refining the MTR model. While early conservative assessments are important for initial safety assessments, they can lead to unrepresentative environmental assessments and issues with public perceptions of radiation risk. However, based on the present dose assessments, the elemental composition of the two types of particles, which influences the particle density and self-absorption, does not seem to contribute significantly to the dose estimates. Based on these results, further environmental impact assessment may be relevant given that 1) there is a high probability of smaller, undetected particles remaining in the marine environment and 2) risk to biota exists where long term to permanent retention of particles is possible, particularly for filter feeders such as blue mussels.

CRediT authorship contribution statement

Ian Byrnes: Conceptualization, Methodology, Formal analysis, Investigation, Data curation, Writing - original draft, Writing - review & editing, Visualization.**Ole Christian Lind:**Conceptualization, Methodology, Formal analysis, Investigation, Resources, Data curation, Writing - original draft, Writing - review & editing, Visualization, Supervision, Project administration.**Elisabeth Lindbo Hansen:**Methodology, Formal analysis, Resources, Data curation, Writing - review & editing.**Koen Janssens:**Methodology, Investigation, Formal analysis, Resources, Data curation, Writing - review & editing.**Brit Salbu:**Conceptualization, Methodology, Resources, Writing - review & editing, Supervision, Project administration, Funding acquisition.

Declaration of competing interest

The authors declare that they have no known competing financial interests or personal relationships that could have appeared to influence the work reported in this paper.

Acknowledgements

This study has been funded by the Research Council of Norway through its Centre of Excellence (CoE) funding scheme (Project No. 223268/F50). The authors are grateful to the Scottish Environmental Protection Agency for providing the samples examined in this study and Deutsches Elektronen-Synchrotron (DESY) for granting beamtime at HASYLAB BL. The authors would like to thank Prof. D.H. Oughton for fruitful discussions on dosimetry, Dr. K. Proost for assistance with micro-XANES measurements, Dr. T. Gävfert for assistance with calibration of the Canberra SPAB15 instrument, and Dr. E. Reinoso-Maset for support on the Bruker M4 Tornado μ-XRF. The authors also thank Karl Andreas Jensen for guidance and support on ICP-MS. Finally, the authors express gratitude to Dr. D. Hamby and the RAMP organization for providing access to the VARSKIN6 code.

Appendix A. Supplementary data

Supplementary data to this article can be found online at https://doi.org/10.1016/j.scitotenv.2020.138488.

References

Anspach, L.J., Hamby, D.M., 2018. Performance of the VARSKIN 5 (v5.3) Electron Dosimetry Model. p. 111.
Aydarous, A.S., Darley, P., Charles, M., 2001. A wide dynamic range, high-spatial-resolution scanning system for radiochromic dye films. Phys. Med. Biol. 46, 1379.
Aydarous, A.S., Charles, M.W., Darley, P.J., 2008. Dose distribution measurements and calculations for Dounreay hot particles. Radiat. Prot. Dosim. 128, 146.
Bolsunovsky, A., Melgunov, M., Chuguevskii, A., Lind, O.C., Salbu, B., 2017. Unique diversity of radioactive particles found in the Yenisei River floodplain. Sci. Rep. 7, 11132.
Bunzl, K., 1997. Probability for detecting hot particles in environmental samples by sample splitting. Analyst 122, 653–656.
Busch, J., Gruehn, R., 1994. Chemischer Transport und Struktur von UNb2O7–einem neuen MM′ 2O7-Typ. Z. Anorg. Allg. Chem. 620, 1066–1072.
Cartwright, P., 1997. Reprocessing of Research Reactor Fuel the Dounreay Option.
CEG, 1990. Comprehensive dismantlement of the Lepse technical floating base. In: Kashka, M. (Ed.), The Contact Expert Group for Nuclear Legacy Initiatives in the Russian Federation (CEG). IAEA, IAEA.
Charles, M.W., 1991. The hot particle problem. Radiat. Prot. Dosim. 39, 39–47.
Choppin, G., Liljenzin, J.-O., Rydberg, J., Ekberg, C., 2013. Radiochemistry and Nuclear Chemistry. Elsevier Science.
Conradson, S.D., Manara, D., Wastin, F., Clark, D.L., Lander, G.H., Morales, L.A., et al., 2004. Local structure and charge distribution in the UO2-U4O9 system. Inorg. Chem. 43, 6922–6935.
Cooper, M.B., Burns, P.A., Tracy, B.L., Wilks, M.J., Williams, G.A., 1994. Characterization of plutonium contamination at the former nuclear-weapons testing range at Maralinga in South-Australia. J. Radioanal. Nucl. Chem. 177, 161–184.
Dale, P., Robertson, I., Toner, M., 2008. Radioactive particles in dose assessments. J. Environ. Radioact. 99, 1589–1595.
Danesi, P.R., Moreno, J., Makarewicz, M., Radecki, Z., 2002. Residual radioactivity in the terrestrial environment of the Mururoa and Fangataufa Atolls nuclear weapon test sites. J. Radioanal. Nucl. Chem. 253, 53–65.
Darley, P.J., Charles, M.W., Fell, T.P., Harrison, J.D., 2003. Doses and risks from the ingestion of Dounreay fuel fragments. Radiat. Prot. Dosim. 105, 49.
Dennis, F., Morgan, G., Henderson, F., 2007. Dounreay hot particles: the story so far. J. Radiol. Prot. 27, A3.
Dounreay Site Restoration Ltd. (DSRL), 2019a. Foreshore Particle Finds.
Dounreay Site Restoration Ltd. (DSRL), 2019b. Murkle Beach Particle Finds.
Dounreay Site Restoration Ltd. (DSRL), 2019c. Sandside Particle Finds.
DPAG, 2008. Dounreay Particles Advisory Group (DPAG) 4th Report. Scottish Environmental Protection AGency (SEPA).
Geckeis, H., Zavarin, M., Salbu, B., Lind, O.C., Skipperud, L., 2019. Environmental chemistry of plutonium. In: Clark, D.L., Geeson, D.A., Hanrahan, R.J. (Eds.), Plutonium Handbook. 4. American Nuclear Society, pp. 1979–2118.
Gesell, T., Baum, J., Scott, B., Hopewell, J., Seltzer, S., Lantz, M., Shore, R., 1999. Biological Effects and Exposure Limits for "Hot Particles". National Council on Radiation Protection and Measurements, Bethesda, Maryland.
Gibson, J., 1997. The Manufacture of MTR Fuel Elements and Mo 99 Production Targets at Dounreay.
Harrison, J., Fell, T., Phipps, A., Smith, T., Ellender, M., Ham, G., Hodgson, A., Wilkins, B., Charles, M., Darley, P., Aydarous, A., 2005. In: Divison, R.P. (Ed.), Health Implications of Dounreay Fuel Fragments: Estimates of Doses and Risks. Health Protection Agency, Oxfordshire, UK.
Henderson, F., Toole, J., Cartwright, P., 2007. The Dounreay Particles Technical Resume. Department of Environmental Protection, United Kingdom Atomic Energy Agency, United Kingdom.
IAEA CRP, 2011. Radioactive Particles in the Environment: Sources, Particle Characterization and Analytical Techniques. International Atomic Energy Agency (IAEA), Vienna, Austria.
International Atomic Energy Agency (IAEA), 2005. Management of High Enriched Uranium for Peaceful Purposes: Status and Trends. IAEA, Vienna.
Jackson, D., Stone, D., Smith, K., Morgan, G., Shimmield, T., 2007. Assessing the environmental risk from hot particles in the vicinity of Dounreay—a case for inaction? J. Radiol. Prot. 27, A111.
Jadernas, D., Gan, J., Keiser, D., Madden, J., Bachhav, M., Jue, J.-F., et al., 2018. Microstructural characterization of as-fabricated and irradiated U-Mo fuel using SEM/EBSD. J. Nucl. Mater. 509, 1–8.
Jaeschke, B.C., Lind, O.C., Bradshaw, C., Salbu, B., 2015. Retention of radioactive particles and associated effects in the filter-feeding marine mollusc Mytilus edulis. Sci. Total Environ. 502, 1–7.
Janssens, K., De Nolf, W., Van Der Snickt, G., Vincze, L., Vekemans, B., Terzano, R., et al., 2010. Recent trends in quantitative aspects of microscopic X-ray fluorescence analysis. Trends Anal. Chem. 29, 464–478.
Kaminski, M.D., 2003. In: USDo, Energy (Ed.), Aqueous Corrosion of Aluminum-Based Nuclear Fuels. Argonne National Laboratory, Argonne, IL.
Kaminski, M.D., Goldberg, M.M., 2002. Aqueous corrosion of aluminum-based nuclear fuel. J. Nucl. Mater. 304, 182–188.
Kaminski, M.D., Dimitrijevic, N.M., Mertz, C.J., Goldberg, M.M., 2005. Colloids from the aqueous corrosion of uranium nuclear fuel. J. Nucl. Mater. 347, 77–87.
Kashparov, V., Yoshchenko, V., Levchuk, S., Tschiersch, J., Wagenpfeil, F., 2000. Application of the method of repeated mixing to non-uniformly contaminated bulky samples. An International Journal Dealing with All Aspects and Applications of Nuclear Chemistry 246, 165–172.
Leenaers, A., Van Renterghem, W., Van Den Berghe, S., 2016. High burn-up structure of U (Mo) dispersion fuel. J. Nucl. Mater. 476, 218–230.
Lind, O.C., 2006. Characterisation of Radioactive Particles in the Environment Using Advanced Techniques. PhD thesis. Norwegian University of Life Sciences, Ås.
Lind, O.C., Salbu, B., Janssens, K., Proost, K., García-León, M., García-Tenorio, R., 2007. Characterization of U/Pu particles originating from the nuclear weapon accidents at Palomares, Spain, 1966 and Thule, Greenland, 1968. Sci. Total Environ. 376, 294–305.
Lind, O.C., Salbu, B., Skipperud, L., Janssens, K., Jaroszewicz, J., De Nolf, W., 2009. Solid state speciation and potential bioavailability of depleted uranium particles from Kosovo and Kuwait. J. Environ. Radioact. 100, 301–307.
Menanteau, F., 2009. SPAB 15 Alpha/Beta Calibration Report. CANBERRA.
Meyer, M.K., Gan, J., Jue, J.F., Keiser, D.D., Perez, E., Robinson, A., et al., 2014. Irradiation performance of U-Mo monolithic fuel. Nucl. Eng. Technol. 46.
National Radiation Protection Board (NRPB), 1997. Assessment of Skin Doses. NRPB, London.
Oughton, D.H., Salbu, B., Brand, T.L., Day, J.P., Aarkrog, A., 1993. Under-determination of SR-90 in soils containing particles of irradiated uranium oxide fuel. Analyst 118, 1101–1105.
Pellet, C., 2004. Estimation of the Contact Frequencies of Critical Groups with Radioactive Particles from the Dounreay Site. RMC Ref. R04-018 (A).
Potter, P., Ray, I., Thiele, H., Wiss, T., 2001. On the Constitution of Dounreay Radioactive Particles, Vol 1 SEM'. United Kingdom Atomic Energy Authorities (UKAEA) Dounreay Internal Report.
Potter, P., Ray, I., Tamborini, G., Theile, H., Wiss, T., 2003. On the Constitution of Dounreay Radioactive Particles Vol 2a'. UKAEA Dounreay Internal Report.
PRAG(D), 2012. Particles Retrieval Advisory Group (Dounreay). Scottish Environmental Protection Agency (SEPA), United Kingdom.
Rest, J., Kim, Y.S., Hofman, G.L., Meyer, M.K., Hayes, S.L., 2006. U-Mo Fuels Handbook. Version 1.0. Argonne National Lab.(ANL), Argonne, IL (United States).
Salbu, B., 2016. Environmental impact and risk assessments and key factors contributing to the overall uncertainties. J. Environ. Radioact. 151 (Pt 2), 352–360.
Salbu, B., Lind, O.C., 2020. Analytical techniques for charactering radioactive particles deposited in the environment. J. Environ. Radioact. 211, 9.
Salbu, B., Krekling, T., Oughton, D.H., Ostby, G., Kashparov, V.A., Brand, T.L., et al., 1994. Hot particles in accidental releases from chernobyl and windscale nuclear installations. Analyst 119, 125–130.
Salbu, B., Krekling, T., Lind, O.C., Oughton, D.H., Drakopoulos, M., Simionovici, A., et al., 2001. High energy X-ray microscopy for characterisation of fuel particles. Nucl. Inst. Methods Phys. Res. A 467, 1249–1252.
Salbu, B., Janssens, K., Lind, O.C., Proost, K., Danesi, P.R., 2003. Oxidation states of uranium in DU particles from Kosovo. J. Environ. Radioact. 64, 167–173.
Salbu, B., Lind, O.C., Kalmykov, S.N., Denecke, M.A., 2011. Radioactive Particles Released into the Environment from Nuclear Events. Springer, Berlin, Heidelberg.
Salbu, B., Kashparov, V., Lind, O.C., Garcia-Tenorio, R., Johansen, M.P., Child, D.P., et al., 2018. Challenges associated with the behaviour of radioactive particles in the environment. J. Environ. Radioact. 186, 101–115.
Schulze, D.G., Bertsch, P.M., 1995. Synchrotron X-ray techniques in soil, plant, and environmental research. In: Sparks, D.L. (Ed.), Advances in Agronomy, Vol 55. 55. Elsevier Academic Press Inc, San Diego, pp. 1–66.
Shevchenko, S.V., 2004. On the uncertainty in activity measurements for samples containing "hot particles". Appl. Radiat. Isot. 61, 1303–1306.
Silva, R.J., Nitsche, H., 2001. Environmental actinide science. MRS Bull. 26, 707–713.

Simon, S.L., Jenner, T., Graham, J.C., Borchert, A., 1995. A comparison of macroscopic and microscopic measurements of plutonium in contaminated soil from the Republic of the Marshall Islands. J. Radioanal. Nucl. Chem. 194, 197–205.

Smith, K., Bedwell, P., 2005. Public Health Implications of Fragments of Irradiated Fuel. Module 3: The Likelihood of Encountering a Fuel Fragment on Sandside Beach. Radiation Protection Division (RPD), Health Protection Agency (HPA) RPD-EA-9-2005.

Soulsby, R.L., Mead, C.T., Wild, B.R., 2006. A Model for Simulating the Dispersal Tracks of Sand-sized Particles in Coastal Areas–"SandTrack". UKAEA, Wallingford, Oxfordshire, UK.

Stewart, A., Cook, G.T., Mackenzie, A.B., 2003. Simulation of Human Stomach and Intenstine Leaching of Dounreay Hot Particles. Scottish Universities Research and Reactor Centre, Scottish Environmental Protection Agency (SEPA).

Strand, P., Beresford, N., Copplestone, D., Godoy, J., Jianguo, L., Saxén, R., et al., 2009. Environmental protection: transfer parameters for reference animals and plants. Ann. ICRP 39, 1–111.

Tamborini, G., 2004. SIMS analysis of uranium and actinides in microparticles of different origin. Micro Trance Anal. 145, 237–242.

Tougait, O., Noel, H., 2004. Stoichiometry of UAl4. Intermetallics 12, 219–223.

Tyler, A.N., Scott, E.M., Dale, P., Elliott, A.T., Wilkins, B.T., Boddy, K., et al., 2010. Reconstructing the abundance of Dounreay hot particles on an adjacent public beach in Northern Scotland. Sci. Total Environ. 408, 4495–4503.

Wilkins, B., Fry, F., Burgess, P., Fayers, C., Haywood, S., Bexon, A., et al., 1998. Radiological Implications of the Presence of Fragments of Irradiated Fuel in the Sub-tidal Zone at Dounreay. NRPB-M1005.